Shaping the heart: Structural and functional maturation of iPSC-cardiomyocytes in 3D-micro-scaffolds

Nicole Silbernagel[a], Arlene Körner[a], Jakob Balitzki[a], Mona Jaggy[b,c], Sarah Bertels[b,c], Benjamin Richter[b,d], Marc Hippler[b,d], Andrea Hellwig[e], Markus Hecker[a,f], Martin Bastmeyer[b,c,g], Nina D. Ullrich[a,f,g,*]

[a] *Institute of Physiology and Pathophysiology, Department of Cardiovascular Research, Heidelberg University, Im Neuenheimer Feld 307, 69120, Heidelberg, Germany*
[b] *Zoological Institute, Cell and Neurobiology, Karlsruhe Institute of Technology (KIT), Fritz-Haber-Weg 4, 76131, Karlsruhe, Germany*
[c] *Institute of Functional Interfaces (IFG), Karlsruhe Institute of Technology (KIT), Hermann-von-Helmholtz-Platz 1, 76344, Eggenstein-Leopoldshafen, Germany*
[d] *Institute of Applied Physics, Karlsruhe Institute of Technology (KIT), Wolfgang-Gaede-Straße 1, 76131, Karlsruhe, Germany*
[e] *Interdisciplinary Center for Neurosciences, Department of Neurobiology, Heidelberg University, Im Neuenheimer Feld 366, 69120, Heidelberg, Germany*
[f] *German Center for Cardiovascular Research (DZHK) Partner Site Heidelberg-Mannheim, Germany*
[g] *Heidelberg-Karlsruhe Research Partnership (HEiKA), Research Bridge (Synthetic Biology), Heidelberg University and Karlsruhe Institute of Technology, Germany*

ARTICLE INFO

Keywords:
iPSC cardiomyocytes
Structure-function
Direct laser writing
3D-micro-scaffolds
Ca^{2+} signaling
Maturation

ABSTRACT

Cardiomyocytes derived from induced pluripotent stem cells (iPSC-CMs) represent the best cell source for cardiac regenerative purposes but retain an immature phenotype after differentiation with significant limitations compared to adult cardiomyocytes. Apart from an incomplete cardiomyocyte-specific structure and micro-architecture, cells show at the level of Ca^{2+} signaling only slow Ca^{2+} release and reuptake properties. Here, we investigated the effect of restructuring single iPSC-CMs in specially designed 3D-micro-scaffolds on cell morphology and Ca^{2+} handling. Using direct laser writing, rectangular-shaped scaffolds were produced and single iPSC-CMs were seeded into these forms. Structural analyses revealed strong sarcolemmal remodeling processes and myofilament reorientation in 3D-shaped cells leading to enhanced clustered expression of L-type Ca^{2+} channels and ryanodine receptors and consequently, to faster Ca^{2+} transient kinetics. Spontaneous beating activity was enhanced and Ca^{2+} handling was more robust compared to non-patterned cells. Overall, our data demonstrate for the first time significant improvement of Ca^{2+} signaling properties in reshaped iPSC-CMs indicative of functional maturation by structural remodeling.

1. Introduction

Cardiac regenerative medicine is confronted with the problem to develop appropriate cells with the ability to compensate for the loss of cardiomyocyte function in the diseased heart [1,2]. Owed to their cardiogenic electrophysiological profile and contractile properties, cardiomyocytes derived from induced pluripotent stem cells (iPSC CMs) represent the ideal cell source to fulfill the task of replacing dysfunctional cardiomyocytes in future therapeutic approaches [3]. In recent years, protocols leading to successful differentiation have been standardized and reproducibly result in a high yield of cardiomyocytes [4]. However, despite the cardiogenic features, iPSC CMs retain a partially immature phenotype after differentiation, and so far it has not been possible to further mature these cells to achieve *in vitro* the complex structural and functional phenotype of adult cardiomyocytes [5]. Even early attempts to mature these cells by implantation into the heart remained unsuccessful in this regard [6,7].

The problem of immaturity of iPSC CMs becomes evident in com parison to adult ventricular cardiomyocytes. Mature cardiomyocytes show a high degree of structural specialization that is directly linked to specific functional properties, especially the cardiac excitation con traction (EC) coupling mechanism [8]. A typical feature of cardio myocytes is their elongated nearly cuboid shape presenting one long axis along which myofibrils are regularly arranged leading to the characteristic striation pattern. Additionally, the sarcolemma shows regular transverse and axial tubular structures, so called TATS or t tu bules, protruding deep into the cell to guide the membrane depolar ization and action potential to inner structures of the myocyte [9]. This

* Corresponding author. Institute of Physiology and Pathophysiology, Department of Cardiovascular Research, Heidelberg University, Im Neuenheimer Feld 307, 69120, Heidelberg, Germany.
E-mail address: nina.ullrich@physiologie.uni-heidelberg.de (N.D. Ullrich).

membrane network comes into close proximity to the sarcoplasmic reticulum (SR), and together they form dyadic structures, the initiation point for EC coupling. Both membranes harbor Ca^{2+} channels, the voltage dependent L type Ca^{2+} channel ($Ca_v1.2$) on the sarcolemmal side, and the Ca^{2+} activated Ca^{2+} release channel or ryanodine receptor (RyR2) at the SR. These Ca^{2+} channels sit opposite each other spaced by about 15–20 nm dyadic cleft and are responsible for the tight regulation of Ca^{2+} induced Ca^{2+} release (CICR), the functional building block of EC coupling [10]. The stringent structural organization is required for the highly spatio temporally synchronized Ca^{2+} release during depolarization and the concerted activation of myofilaments for efficient contraction. Disruption of this microarchitecture leads to reduced EC coupling efficiency and loss of synchronization of myofilament activation resulting in weaker contraction and eventually heart failure [11,12].

In comparison, iPSC CMs present neither this specific cell shape, nor do they produce the characteristic sarcolemma invaginations [13]. The lack of the regular cell architecture with unorganized distribution of myofibrils results in uncoordinated contraction. In addition, one hallmark of iPSC CM immaturity is their spontaneous beating activity caused by spontaneous depolarizations and Ca^{2+} transients leading to contractions. This automaticity is reminiscent of prenatal native cardiomyocytes, which remain spontaneously active for some time after birth (duration is species dependent). The exact mechanisms underlying automaticity may involve immature Ca^{2+} handling, which might be related to the expression of premature protein isoforms involved in control of Ca^{2+} homeostasis [14]. However, so far it has not been possible to overcome the stage of spontaneous activity *in vitro*.

The mechanisms of cardiomyocyte maturation remain poorly understood. Moreover, a unified definition of maturation is still missing. Ultimately, the new cardiomyocytes will have to provide the same functional complexity in terms of EC coupling control, Ca^{2+} handling, force production and humoral response as native cardiomyocytes before they can be used for therapeutic applications. With respect to cardiac development, a multitude of different factors may influence myocyte maturation. In principle, these factors can be grouped into biophysical, biochemical or biological cues. Accordingly, previous studies have involved electrical and mechanical stimulation, small molecules, genetic approaches, co culture or implantation (just to mention a few) to trigger further maturation of iPSC CMs with focus on either structural or functional properties [4,15–17].

Here, we tested the hypothesis that structural remodeling of single iPSC CMs by 3D micro scaffolds into the style of adult cardiomyocytes leads to improved and robust Ca^{2+} handling in these cells. For this approach, using the technique of direct laser writing (DLW) we have produced 3D micro scaffolds in the shape of cuboids (and hexagons as control) for single cell growth. Single cells grown within these scaffolds were analyzed and compared with non patterned cells using a broad range of different techniques. Our data demonstrate that the induced elongated cell shape has tremendous influence on cell micro architecture and membrane properties, modifies protein expression and distribution patterns and leads to robust Ca^{2+} handling during spontaneous and triggered activity. Therefore, we propose that specific control of cell morphology can trigger structural and functional maturation processes in iPSC CMs and improve the cardiogenic phenotype at the level of EC coupling.

2. Methods

2.1. Cell models

Murine induced pluripotent stem cell derived cardiomyocytes (iPSC CMs, Cor.At®, Axiogenesis/Ncardia, Cologne, Germany) were delivered and stored in liquid nitrogen until use. After defrosting, cells were cultured as previously described [18]. Briefly, cells were seeded in glass bottom dishes (35 mm, MatTek Corporation, Ashland, MA, USA) or glass coverslips with DLW printed 3D structures (scaffolds, see below). All culture surfaces were coated with a mixture of laminin and fibronectin in PBS (1:1:100) overnight at 37 °C and cells were seeded at a density of 2×10^4 cells per dish. For the selection of cardiomyocytes and elimination of undifferentiated cells or non cardiomyocytes, cells were treated with puromycin (1 μg/ml) for selection of cardiac specific cells. The pac gene expression for puromycin resistance was under control of the cardiomyocyte specific α myosin heavy chain (αMHC) promoter. After 48 h, cells were switched to puromycin free CorAt® medium according to the manufacturer's protocols. Cells were incubated at 5% CO_2 and 37 °C with CorAt® medium and used within 3 weeks after defrosting.

Adult ventricular cardiomyocytes were freshly isolated from mouse hearts (wild type C57BL/6J, 2 month old) as described previously [19]. Briefly, hearts were excised, cannulated and retrogradely perfused with (in mM) 140 NaCl, 5.4 KCl, 1.1 $MgCl_2$, 1 Na_2HPO_4, 5 HEPES, and 10 glucose (pH 7.4 with NaOH) on a Langendorff apparatus. Cardiomyocytes were enzymatically dissociated using collagenase (1 mg/ml, Worthington Biochemical Corp., Lakewood, NJ, USA) and protease (50 μg/ml, Sigma Aldrich Chemistry, Munich, Germany) to obtain single cells. After dissociation, cells were directly fixed and prepared for immunofluorescence or ultrastructural analyses. All experimental procedures were performed according to the guidelines of the local animal care committee (Regierungspräsidium Karlsruhe, Germany) and conformed to the Guide for the Care and Use of Laboratory Animals by the US National Research Council.

2.2. 3D micro scaffold fabrication

2.2.1. Coverslip silanization

Prior to usage in the DLW process and replication, glass coverslips were silanized in order to enhance the adhesion of the photoresist to the substrate. The glass coverslips were first cleaned with isopropanol (Carl Roth, Karlsruhe, Germany) and incubated in a Plasma Prep5 plasma cleaner (GaLa Instruments, Micro Precision Calibration Inc., Nijmegen, Netherlands) for 10 min to produce a hydrophilic surface. This step was followed by treatment with 1 mM 3 (trimethoxysilyl)propyl methacrylate (≥98%, Sigma Aldrich) in toluene (Carl Roth, Karlsruhe, Germany) for 60 min at room temperature (RT). The coverslips were then rinsed in distilled water and dried with nitrogen gas.

2.2.2. Direct laser writing (DLW)

For the fabrication of the 3D micro structures, a commercially available DLW system (Photonic Professional GT, Nanoscribe GmbH, Eggenstein Leopoldshafen) equipped with a 25 × NA (numerical aperture) = 0.8 oil immersion objective was employed. A liquid photoresist composed of the monomer pentaerythritol triacrylate (PETA, Sigma Aldrich) with 2% w/w of photoinitiator Irgacure 819 (BASF, Ludwigshafen, Germany) was polymerized via two photon absorption using a frequency doubled erbium fiber laser with a center wavelength of 780 nm and a pulse length of 90 fs (Fig. 1A) [20]. Typical average laser powers were 20–30 mW (in front of the microscope lens) and the typical scanning velocity was 50 mm/s 3D structures in the shape of cuboids ($22 \times 55 \times 20$ μm^3) and hexagons ($6 \times 22 \times 20$ μm^3), both with a wall thickness of 1–2 μm, were produced, several repeats were printed onto the same coverslip. The 3D structures were developed in a 1:1 (v/v) mixture of methyl isobutyl ketone (MIBK, Carl Roth, Karlsruhe, Germany) and isopropanol for 10 min and subsequently dried with nitrogen. 3D scaffolds were sputtered with gold and examined at a scanning electron microscope (Fig. 1B). For cell experiments, the 3D scaffolds were sterilized with 70% (v/v) ethanol and subsequently dried for 30–60 min under UV light. They were then washed with PBS. To promote cell adhesion the substrates were coated with extracellular matrix proteins diluted in PBS (see above).

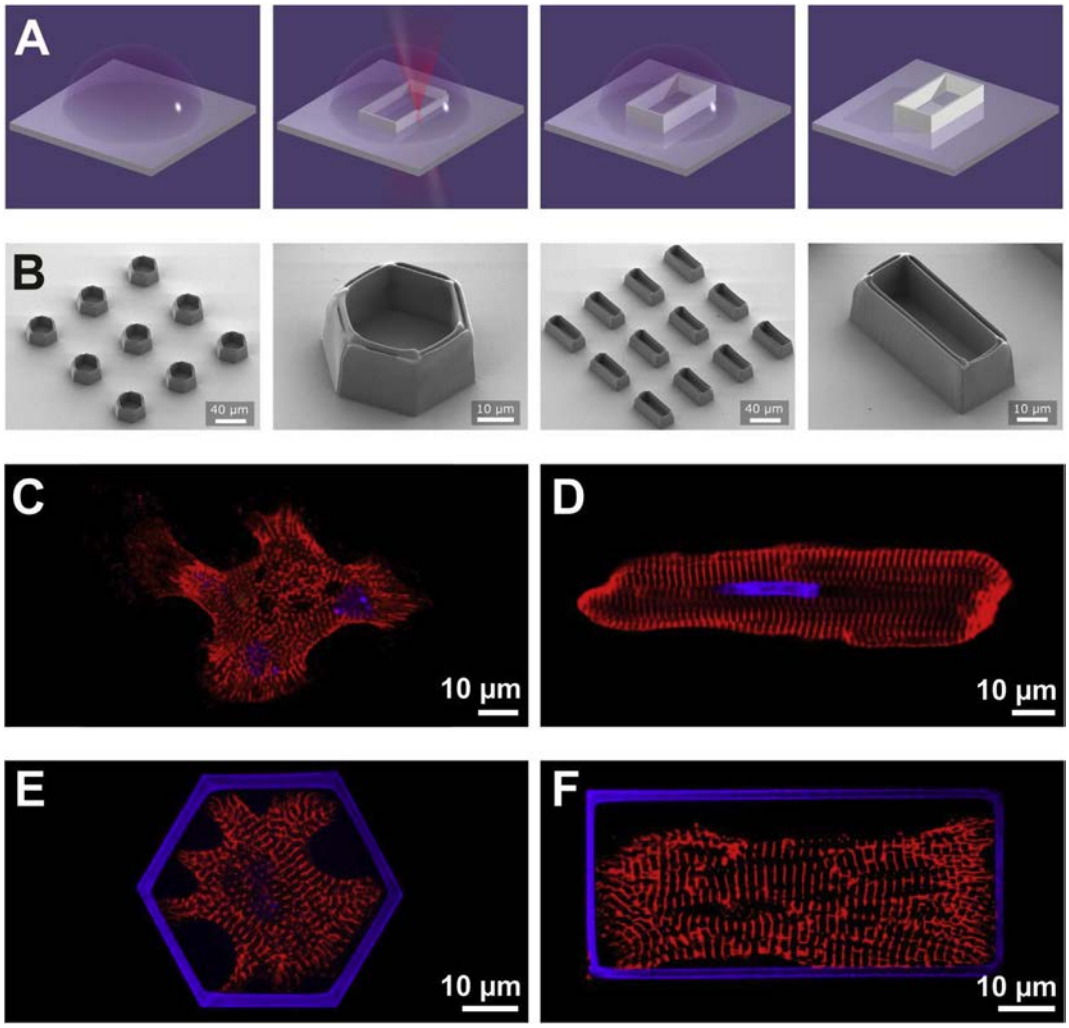

Fig. 1. 3D-scaffolds and their influence of on cell morphology. A) Schematic drawing of the single steps of the direct laser writing (DLW) technique to produce 3D-scaffolds for reshaping individual iPSC-CMs: from *left* to *right*: a drop of liquid PETA is put on a glass coverslip; at the focal plane of the laser beam, the monomers start to polymerize and build solid structures of the desired shapes. The remaining liquid is washed off at the end of the writing procedure. **B)** Resulting 3D-scaffolds in either hexagonal (*left* images) or cuboid shape (*right* images) are shown at two different magnifications; several structures are printed onto the same coverslip to enhance seeding success during cell dropping. **C–F**) Sarcomeric α-actinin (red, indicating Z-lines) and nuclear stainings by DAPI (*blue*) of non-patterned (NP) iPSC-CMs (**C**), freshly isolated adult cardiomyocyte (**D**), and iPSC-CMs grown in hexagonal (**E**) or cuboid 3D-scaffolds (**F**). Note the almost parallel alignment of myofibrils indicated by regular Z-band stainings perpendicular to the long axis of the cuboid. Autofluorescence of the scaffold polymer is visible in *blue*.

2.3. Transmission electron microscopy (TEM)

iPSC CMs grown in rectangular shaped 3D scaffolds and NP cells were collected and processed from 11 individual cultures. Cells were washed with PBS containing 3 µM blebbistatin to stop cells from con tracting and to induce myofibril relaxation. Cells were fixed with 4% glutaraldehyde in 0.1 M sodium cacodylate buffer containing 2% polyvinylpyrrolidone at pH 7.5. For enhancement of membrane con trasting, samples were incubated in alkaline diaminobenzidine (DAB) medium for 30 min and postfixed with 1.5% osmium tetroxide in 0.1 M sodium cacodylate buffer. After washing, cells were contrasted with 1% uranyl acetate, dehydrated by a graded ethanol series and embedded in glycidether 100 based epoxy resin. Semithin sections were stained with a methylene blue/azure II solution (modified after Richardson et al. [21]) and cells were selected for the following detailed examination. Ultrathin sections were cut with a Reichert Ultracut S ultramicrotome (Leica, Vienna, Austria) and stained with lead citrate for further ana lysis by electron microscopy (Zeiss EM 10 CR) at an acceleration vol tage of 60 kV. Images were obtained with technical help from the team of Hilmar Bading, Department of Neurobiology at Heidelberg Uni versity. TEM images were evaluated using ImageJ (NIH Image, free software, Bethesda, MD, USA).

2.4. Immunocytochemistry

iPSC CMs were grown on non patterned 2D surfaces, in rectangular or hexagonal 3D micro scaffolds, respectively. Cells were fixed in 4% paraformaldehyde (ThermoFisher Scientific, Waltham, MA, USA), blocked and permeabilized with 0.1% TritonX 100 and 1% bovine serum albumin in PBS for 10 min at RT. Cells were selectively labeled with primary antibodies for α actinin (mouse monoclonal, 1:500, A7811, Sigma Aldrich or rabbit polyclonal, 1:500, ab90776, Abcam, Cambridge, MA, USA), L type calcium channel $Ca_v1.2$ (rabbit poly clonal, 1:200, AB10515, MerckMillipore, Darmstadt, Germany), rya nodine receptor RYR2 (mouse monoclonal, 1:200, ab2827, Abcam), inositol 1,4,5 trisphosphate receptor IP_3R (goat polyclonal, 1:200, sc 26386, Santa Cruz Biotechnology, Dallas, TX, USA) and the sarco en doplasmic reticulum Ca^{2+} ATPase SERCA2 (mouse monoclonal, 1:400, ab2861, Abcam). Appropriate secondary antibodiesconjugated to Alexa Fluor dyes of different excitation emission spectra were used (1:500, ThermoFisher Scientific). Nuclei were stained with 4′,6 diamidino 2 phenylindole (DAPI) present in the mounting medium (Fluoroshield

F6057, Sigma Aldrich). Each staining was repeated at least 5 times in individual cultures of iPSC CMs, and from each staining, at least 10 cells were imaged and analyzed. Images were taken on a laser scanning confocal microscope (Leica SP8, Mannheim, Germany) using 63x oil immersion objective (1.4 NA). Samples were excited in sequential scans using laser excitation at 405 nm, 488 nm, 552 nm and 638 nm. Emission spectra were selected via tunable filters and emission was detected using photomultiplier tubes (PMT) and hybrid detectors (HyD). High resolution images were taken using the acquisition software LAS X (by Leica). Images were further processed in ImageJ. Using a special plugin of ImageJ (TTorg) designed to measure t tubular distances [49], α ac tinin stainings indicating sarcomeric Z discs were analyzed and sarco mere lengths calculated.

2.5. Live cell imaging

For all live cell imaging experiments, standard bath solution was cardiac Tyrode's solution containing (in mM): NaCl 140, KCl 5.4, $CaCl_2$ 1.8, $MgCl_2$ 1.1, HEPES 5, glucose 10, pH 7.4.

2.5.1. Plasma membrane staining

Cells of either culturing condition were stained with the fluorescent membrane dye di 8 ANEPPS for live imaging. Cells were incubated in 0.5 μM di 8 ANEPPS (ThermoFisher Scientific) in normal Tyrode's so lution for 5 min at RT without light exposure. Just before live imaging, cells were washed twice in Tyrode's solution for removal of any un bound dye. To avoid contractions during imaging, 3 μM blebbistatin (1760, Tocris Bio Techne, Wiesbaden Nordenstadt, Germany) was added to the bath solution.

2.5.2. Calcium imaging of spontaneous and triggered activity

Spontaneous Ca^{2+} release activity of iPSC CM was recorded using the Ca^{2+} sensitive fluorescent dye Fluo4 (from a 10 mM Fluo4 AM stock solution dissolved in DMSO, ThermoFisher Scientific). Cells were loaded with 3 μM Fluo4 diluted in Tyrode's solution for 30 min at RT. Cells were recorded 10 min after washing with Tyrode's solution for de esterification. Global superfusion with fresh Tyrode's solution at the speed of 1 drop/s avoided depletion of nutrients. Spontaneous Ca^{2+} transients were recorded using linescan imaging. Additional experi ments were performed while pacing cells with a field stimulator (Myopacer, IonOptix, Dublin, Ireland). Using a stimulation amplitude of 15 V and a frequency of 1 Hz, cells were paced 10 times. During and after pacing, linescan images were recorded to capture spontaneous and triggered Ca^{2+} transients.

Full frame and linescan images were taken on a laser scanning confocal microscope (Olympus Fluoview FV1000, Hamburg, Germany) using a 60x water immersion objective (1.2 NA). For acquisition of fast Ca^{2+} signals, linescans were collected at 8 μs/pixel, 4.7 m s/line and 8000 lines/image. Excitation wavelength was 473 nm and fluorescence emission was collected between 490 nm and 545 nm. Linescans were analyzed in ImageJ. Analysis comprised frequency of spontaneous Ca^{2+} transients, temporal delay between triggered and spontaneous Ca^{2+} transients, Ca^{2+} transient kinetics (full duration at half maximum FDHM, rise time constant τ, decay time constant k). Caffeine induced (10 mM) Ca^{2+} transients served as SR Ca^{2+} load controls and were analyzed to calculate fractional release and SERCA contribution of Ca^{2+} reuptake after release [22]. All experiments were performed at RT.

2.6. Data analysis and statistics

Imaging data were analyzed using ImageJ. Data were further pro cessed in OriginPro® (OriginLab Corporation, Northampton, MA, USA) for statistical analysis and graph design. Illustrations and figures were produced in CorelDraw X6 (Corel Corp., Ottawa, Canada). For data analysis, mean, standard error of mean (SEM), standard deviation (SD) and coefficient of variation were calculated, n equals number of ana lyzed cells. Statistical significance was tested using two sample Student's *t* test and one way ANOVA. Significant differences in data sets are indicated by * for $P < 0.05$, ** for $P < 0.01$ and *** for $P < 0.001$.

3. Results

Cells growing in 3D micro scaffolds show structural reorganization of subcellular microarchitecture. When iPSC cardiomyocytes (iPSC CMs) grow on a planar surface like conventional coverslips or the bottom of cell culture dishes, they are flattened and do not reveal any defined axis formation or shape. As a consequence, the subcellular ar rangement of intracellular organelles and the myofilaments mostly appear in no particular organization. If myofibrils are formed, they are not regularly arranged. In contrast, freshly isolated adult ventricular cardiomyocytes appear as almost cuboid shaped large cells with a clearly visible longitudinal axis, along which the cells contract after stimulation. Strict parallel alignment of myofibrils enables optimal force production during contraction as compared to cells with myofi brils that are not organized and span into different directions. To in vestigate the effects of cell shape on their subcellular structural orga nization, iPSC CMs were seeded into 3D scaffolds prepared by DLW (Fig. 1A) of hexagonal and rectangular forms (Fig. 1B) and cultured for several days. Cuboid 3D scaffolds were prepared based on the rectan gular structure of adult cardiomyocytes with dimensions that were previously published and successfully used in 2D stamping techniques with premature neonatal cardiomyocytes. Optimal length to width ratio of 2D printed rectangles for the development of cellular anisotropy in single neonatal cardiomyocytes was reported to be above an aspect ratio of 2:1 [50]. We have optimized the dimensions for the technique of direct laser writing (22×55 μm, 20 μm height) so that during seeding, one spheric cells would drop into each of the 3D shapes, settle down and adhere to the growth surface and scaffold walls, elongate and also grow in height. For direct control experiments, hexagonal 3D shapes of similar surface area and height ($s = 22$ μm, $h = 20$ μm) were designed that do not permit any elongation of the cells during culture. Instead, the cells keep a similar shape as if they were grown without any given pattern, but within a confined surface area. Cells adopted the form of the given 3D scaffolds within 2 3 days. After 5 days in culture, iPSC CMs were fixed and immunostained to visualize the orientation of myofibrils. iPSC CMs growing on a uniformly coated 2D surface, re ferred to as non patterned, NP, were stained for the sarcomeric Z line protein α actinin, which is oriented perpendicular to the long axis of the myofibrils (Fig. 1C). For comparison, a single ventricular cardio myocyte freshly isolated from adult heart revealed regularly spaced and parallel α actinin signals indicating precise alignment of myofibrils along the long axis of the myocyte (Fig. 1D). Orientation of myofibrils in iPSC CMs grown in hexagonal 3D scaffolds (Fig. 1E) strongly re sembles the diffuse distribution pattern in NP cells. In contrast, cells growing in cuboid 3D scaffolds show a remarkable reorganization with strong parallel alignment of their myofibrils as indicated by corre sponding α actinin stainings (Fig. 1F) similar to the sarcomere pattern of adult cardiomyocytes. Analysis of the sarcomere lengths of NP and reshaped cells using α actinin staining representative for the Z discs revealed no significant differences in the sarcomeric distances. Sarco mere lengths amounted to 1.70 ± 0.07 μm in NP cells ($n = 5$), 1.69 ± 0.02 μm in cuboid cells ($n = 7$) and 1.64 ± 0.05 μm in hex agonal cells ($n = 7$) ($P > 0.05$, using one way ANOVA), demonstrating that there was no effect of reshaping on myofibril organization at the level of sarcomere length. These initial experiments convincingly de monstrate that forcing single iPSC CMs to grow in rectangular shapes leads to structural reorganization of myofilaments and orientation of contractile myofibrils reminiscent of mature cardiomyocytes.

Structural remodeling leads to membrane invaginations. Apart from their unspecific natural shape, iPSC CMs also differ from adult

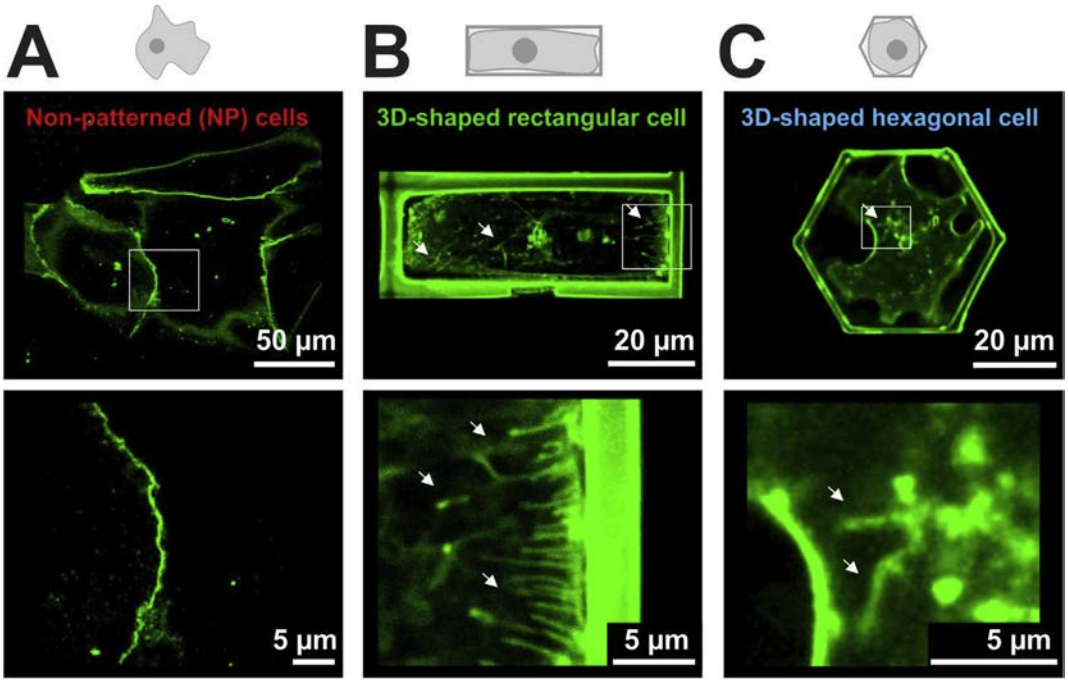

Fig. 2. Structural remodeling of iPSC-CMs in 3D-scaffolds. Live cell imaging of the sarcolemma using di-8-ANEPPS in two magnifications in NP cells (**A**), rectangular- (**B**) and hexagonally-shaped iPSC-CMs (**C**). Note the strong membrane invaginations in 3D-shaped cells compared to NP cells. White boxes in the upper rows indicate area of magnification. White arrows indicate location of membrane invaginations.

cardiomyocytes by the lack of t tubules. Using the fluorescent mem brane dye di 8 ANEPPS, the sarcolemmal structures were recorded in live cells. Under these experimental conditions, the fluorescent signal indicates the plasma membrane outlining the cells (Fig. 2). In NP iPSC CMs growing on uniformly coated 2D surfaces, no membrane foldings or invaginations were present (Fig. 2A). In contrast, cells grown within 3D scaffolds revealed fine tubular membrane invaginations protruding from the cell periphery or from the top surface deep into the cell (cu boids in Fig. 2B, n = 5, and hexagons in Fig. 2C, n = 3). Interestingly, rectangular shaped cells showed strong tubular invaginations mainly from the end poles of the cell, indicative of early stages of membrane remodeling towards the formation of t tubules.

Ultrastructural analysis of rectangular shaped iPSC CMs revealed sarcolemmal t tubule like structures. The presence of t tubule like structures was further investigated by electron microscopy. In com parison with adult cardiomyocytes, which revealed a well organized microarchitecture, densely packed mitochondria between parallel aligned myofibrils and regular t tubules at the level of the Z lines (Fig. 3A), NP iPSC CMs exhibited chaotic arrangement of myofilaments and mitochondria with no recognizable t tubular structures. In rectan gular shaped iPSC CMs grown in 3D micro scaffolds, however, the sarcomeric units were more regularly organized in clearly structured units and parallel to the scaffold wall (Fig. 3A and B). Furthermore, in some specimen, regular t tubule like and even dyadic structures of sarcolemmal and adjacent SR membranes could be identified near the Z line (Fig. 3B). This is the first experimental evidence that structural remodeling by change of cell shape leads to t tubule like membrane invaginations.

Reshaping of cells leads to increased cell height. In addition to the subcellular reorganization of myofilaments, membrane compartments and other organelles, culture of iPSC CMs in scaffolds with limited space may force the cells to grow in height. Single cells were analyzed by confocal imaging in the z dimension and cell height was measured. In contrast to NP cells (8.0 ± 0.6 µm, n = 10), iPSC CMs in rectangular or hexagonal shapes exhibited significantly increased cell height (Fig. 3C; 16.6 ± 1.4 µm, n = 10; 17.4 ± 1.0 µm, n = 10, respec tively). The increase in height may enable reorganization of organelles and development of new microcompartments and their specific spatial relation with direct consequences on cardiomyocyte function.

Expression pattern of Ca^{2+} handling proteins reveals reorganization in rectangular shaped iPSC CMs. In the next step, we wanted to in vestigate the effect of structural remodeling on the Ca^{2+} regulatory mechanisms in iPSC CMs. For this purpose, we first looked at the ex pression of relevant proteins that are known to be critical for Ca^{2+} handling in cardiomyocytes. The tested proteins comprised the L type Ca^{2+} channel ($Ca_v1.2$) as key Ca^{2+} influx pathway for EC coupling, the RyR2, which is the most important Ca^{2+} release channel in the SR, but also the inositol 1,4,5 trisphosphate receptor (IP_3R), which is known to be expressed in immature cardiomyocytes, and SERCA, the main Ca^{2+} ATPase relevant for refilling the SR after Ca^{2+} release. In principle, iPSC CMs express all key Ca^{2+} handling proteins needed for the control of contraction. Fig. 4A illustrates the expression of these proteins in NP iPSC CMs. Interestingly, despite the absence of well developed t tu bules, $Ca_v1.2$ expression was closely linked to α actinin expression re sulting in a characteristic striation pattern hinting toward the location of costameres. The strong expression of IP_3R indicates a possible con tribution of IP_3 mediated Ca^{2+} release to Ca^{2+} cycling in these cells, reminiscent of immature native cardiomyocytes. SERCA protein ex pression revealed mostly a dotted and diffuse expression pattern, al though regionally small areas of striation pattern could be detected indicating the SR organization along myofibrils. RyR2 revealed strong expression levels in all iPSC CMs (Fig. 4B). In cells grown in hexagonal 3D scaffolds, small areas were discernible, where dotted RyR2 expres sion followed a regular striped expression pattern. However, in cells grown in rectangular 3D scaffolds, RyR2 expression was highly orga nized in a striation pattern indicative for a well developed SR network. The improvement of RyR2 expression was demonstrated in line profiles showing the regular spacing of fluorescence peaks in cuboid cells compared to the punctate expression pattern in hexagonal cells, which also indirectly indicate the arrangement of the SR (Fig. 4B). Since $Ca_v1.2$ and RyR2 are the main key players determining EC coupling in cardiomyocytes, shape dependent changes in expression pattern were investigated in double stainings. Representative expression patterns of $Ca_v1.2$ and RyR2 in NP and cuboid cells are depicted and analyzed in

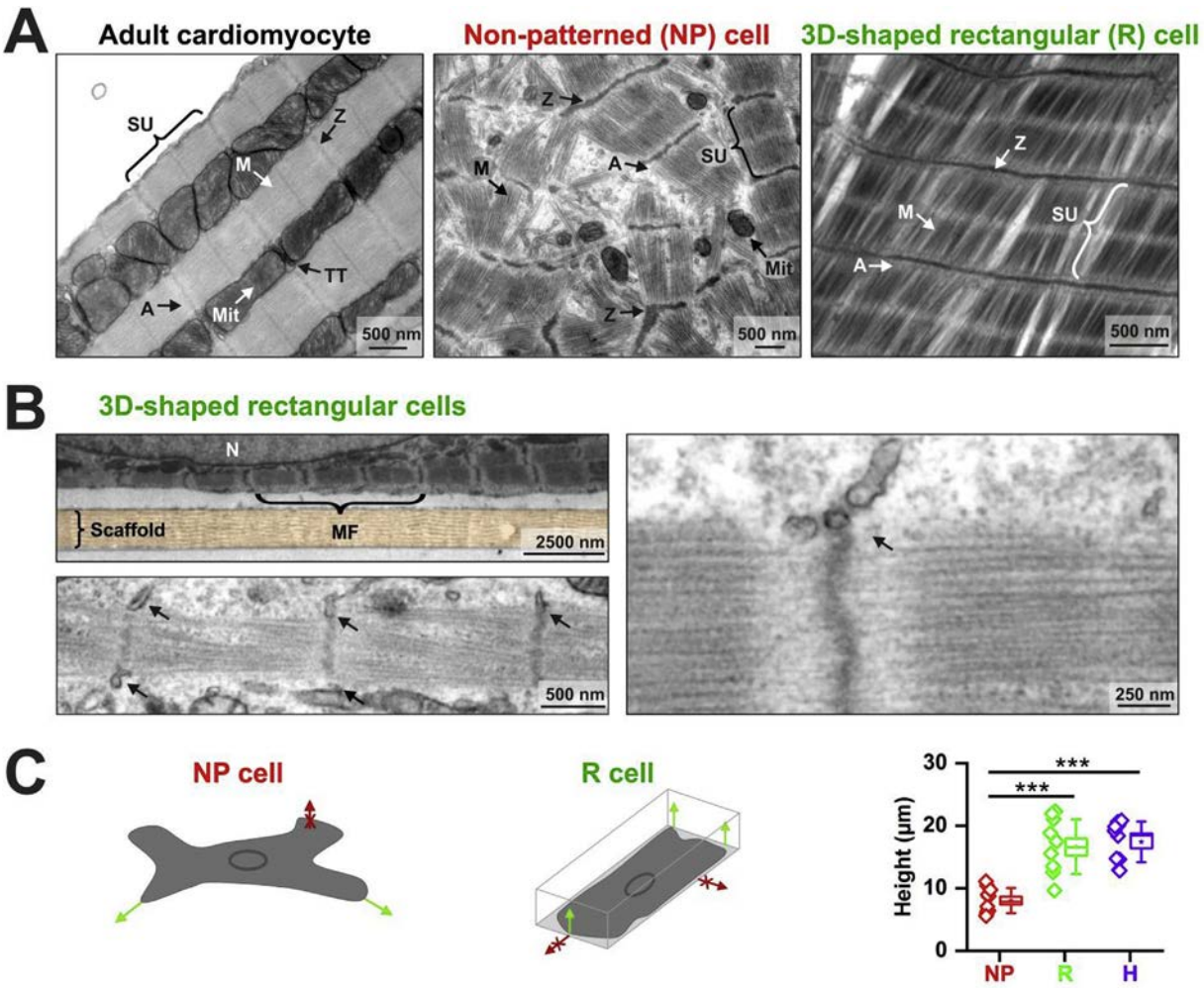

Fig. 3. Ultrastructural changes of cardiomyocytes by structural remodeling. A) *from left to right:* sarcomeric units (SU) in an adult cardiomyocyte, NP iPSC-CM, and iPSC-CM grown in a cuboid scaffold (R) showing parallel alignment of myofibrils. **B)** *Left top:* detail of cell membrane next to scaffold wall; *left bottom:* regular arrangement of tubular structures (indicated by arrows) along Z-lines of myofibrils. *Right image:* detail of sarcolemmal and sarcoplasmic reticulum tubules (arrow) near Z-line. A, actin filaments; M, myosin filaments; MF, myofibril; Mit, mitochondrium; N, nucleus; SU, sarcomeric unit; TT, transverse tubule; Z, Z-line. **C)** Schematic illustration (*left*) and quantitative analysis (*right*) of iPSC-CM growth on NP surfaces and within 3D-shaped rectangular structures (R). Growth direction is indicated by green arrows (→) whereas growth limitations are marked in red (>><<). Analysis of cell height in NP, R and hexagonal (H) iPSC-CMs.

images shown in Fig. 4C. While $Ca_v1.2$ expression showed numerous areas of regular striation pattern with a peak to peak distance of ~1.7 µm, the length of one sarcomere, RyR2 expression was mainly dotted in NP cells, as reflected by a low degree of fluorescent signal overlap. In contrast, in cuboid shaped iPSC CMs, there is significant degree of overlap of peak expression of both Ca^{2+} channels, exhibiting strong regular striation pattern across the cell and perpendicular to the long axis and myofibril orientation. Line profiles of RyR2 and $Ca_v1.2$ expression confirmed the spatial synchronization and clustering with peak to peak distances corresponding to the length of sarcomeric units. These data indicate reorganization of $Ca_v1.2$ and RyR2 Ca^{2+} channels relative to each other in rectangular shaped cells bringing them in close proximity. In the next set of experiments, we investigated whether the structural rearrangement also resulted in functional adaptations of Ca^{2+} handling in 3D shaped iPSC CMs with a higher degree of orga nization.

Structural reorganization significantly influences Ca^{2+} handling in iPSC CMs. To investigate the effect of shape on function, spontaneous Ca^{2+} transients were imaged and analyzed. For this set of experiments, cells were grouped according to 4 different phenotypes: cells grown on non patterned 2D surfaces without any defined shape (NP), so called shaped cells (S), which were NP cells that occasionally adopted a longitudinal shape (< 2% of all NP cells), and cells grown in rectangular (R) or hexagonally (H) shaped 3D scaffolds. Cells were loaded with the Ca^{2+} sensitive fluorescent indicator Fluo4 and confocal linescan images were recorded over the duration of 6 s. Representative linescans and line profiles from the 4 distinct phenotypes are sum marized in Fig. 5A. The frequency as well as the Ca^{2+} transient dy namics in terms of FDHM were analyzed. Frequency of spontaneous depolarizations and Ca^{2+} transients was significantly faster in all shaped cells and highest in cells grown within 3D scaffolds (Fig. 5B). Along the same lines, Ca^{2+} transients of NP cells were significantly slower in their decay kinetics compared to shaped cells (Fig. 5C). In contrast to NP cells, the FDHM was significantly reduced in S, R and H cells. However, no major differences were detected between R and H cells. Both, faster frequency and FDHM are indicative for a higher ef ficiency of Ca^{2+} handling in shaped iPSC CMs.

iPSC CMs grown in scaffolds show significant improvement in Ca^{2+} reuptake mechanisms. To further explore the functional consequences of cell growth in 3D scaffolds on Ca^{2+} homeostasis, iPSC CMs were exposed to electric field stimulation. For this last set of experiments, two protocols were applied. First, cells were paced at 1 Hz for 10 times, and confocal linescans of Fluo4 signals were collected during the last 5 pulses to record steady state Ca^{2+} transients and recovery of sponta neous activity after pacing. Second, directly after pacing, 10 mM caf feine was applied to empty the SR Ca^{2+} store. Again, the time to

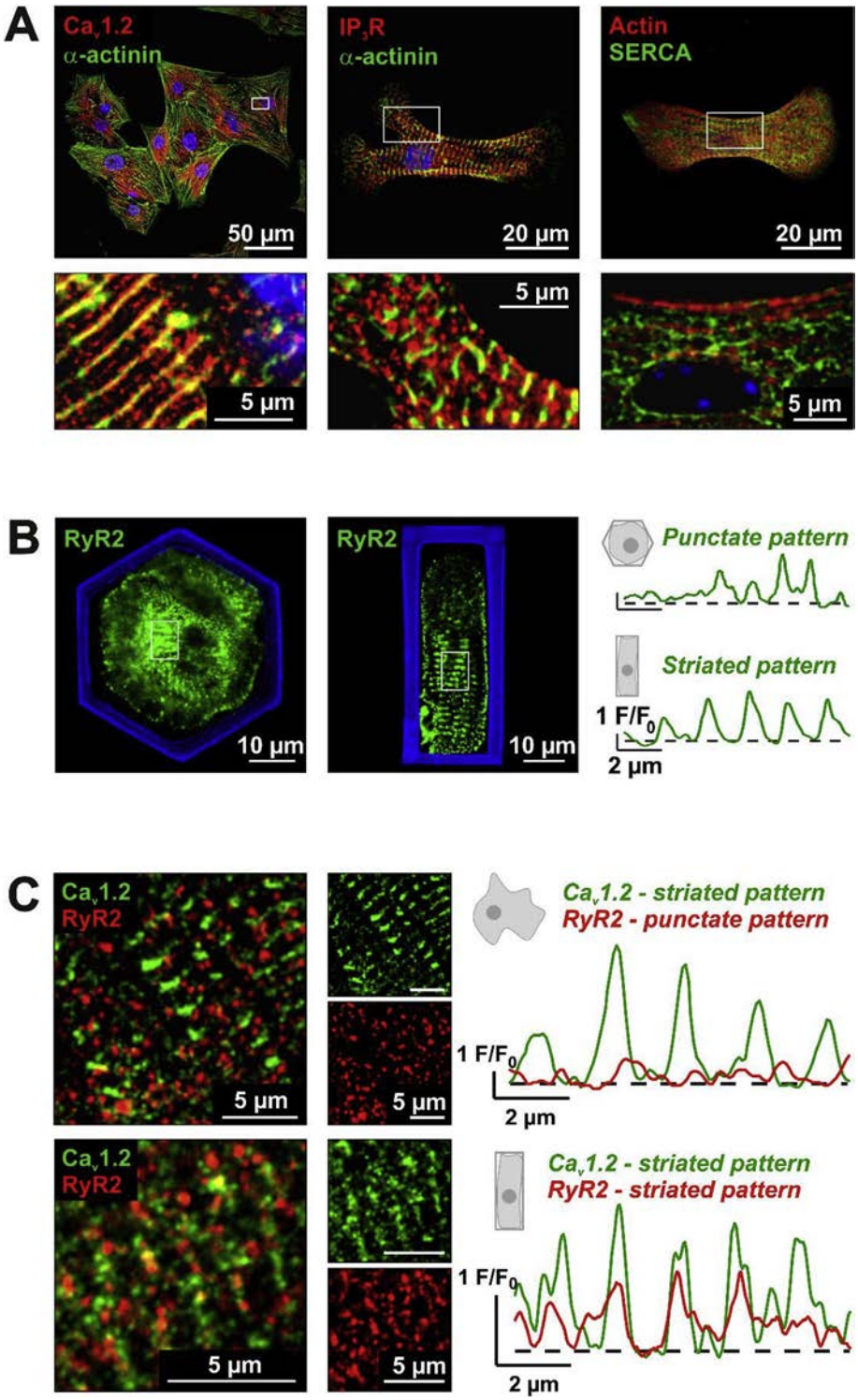

Fig. 4. Expression patterns of Ca^{2+} handling proteins in iPSC-CMs relative to sarcomeric α-actinin: **A)** *left*: L-type Ca^{2+} channel $Ca_v1.2$ (*red*) and α-actinin (*green*), *middle*: IP_3-receptor (*red*) and α-actinin (*green*), *right*: SERCA2 (*green*) and actin (red). White boxes indicate magnified areas of the images shown below. **B)** RyR2 staining in 3D-shaped hexagonal (*left*) and cuboid iPSC-CMs (*center*) with corresponding line profiles of RyR2 expression pattern and its new organization in rectangular cells (*right*). **C)** $Ca_v1.2$ (*green*) and RyR2 (*red*) expression pattern in NP cells (*top images*) and in rectangular shaped cells (*bottom images*). Note the reorganization of $Ca_v1.2$ (*green*) and RyR2 (*red*) from a punctate expression pattern of RyR2 in NP cells to the new location near $Ca_v1.2$ in rectangular 3D-shaped iPSC-CMs. Overlay images are shown in large, separate channels in small images. Line profiles on the right side indicate clustering of $Ca_v1.2$ and RyR2 especially in cuboid iPSC-CMs.

recovery of spontaneous activity was assessed. Fig. 6A illustrates the details of the experimental protocols. Three groups of different cell phenotypes were investigated: NP cells growing on 2D surfaces (*red*), cells grown in rectangular (R, *green*) and hexagonal (H, *blue*) 3D scaf folds. Fig. 6B D shows representative linescan images and line profiles of the different cell shapes. The frequency of Ca^{2+} transients after re start of spontaneous activity is summarized in Fig. 6E. In accordance with our previous analysis (Fig. 5), we could observe that after pacing, NP cells had a lower frequency of spontaneous Ca^{2+} transients than R or H cells in 3D scaffolds. In Fig. 6F, the pause after pacing until the restart of spontaneous Ca^{2+} transients was evaluated. Intermission of R or H iPSC CMs was significantly reduced until restart of spontaneous activity. However, 20% of NP iPSC CM did not reach any recovery of spontaneous activity after pacing and therefore no Ca^{2+} transients were detectable and no duration of pause could be defined in the recorded linescans (data not shown). Next, the number of Ca^{2+} transients (peaks) after caffeine dependent Ca^{2+} depletion of the SR was counted for the duration of the linescan recording (20 s, Fig. 6G). Both, R and H iPSC CMs presented significantly more Ca^{2+} transients than NP cells. Next, triggered Ca^{2+} transients were analyzed for their kinetics. NP cells had

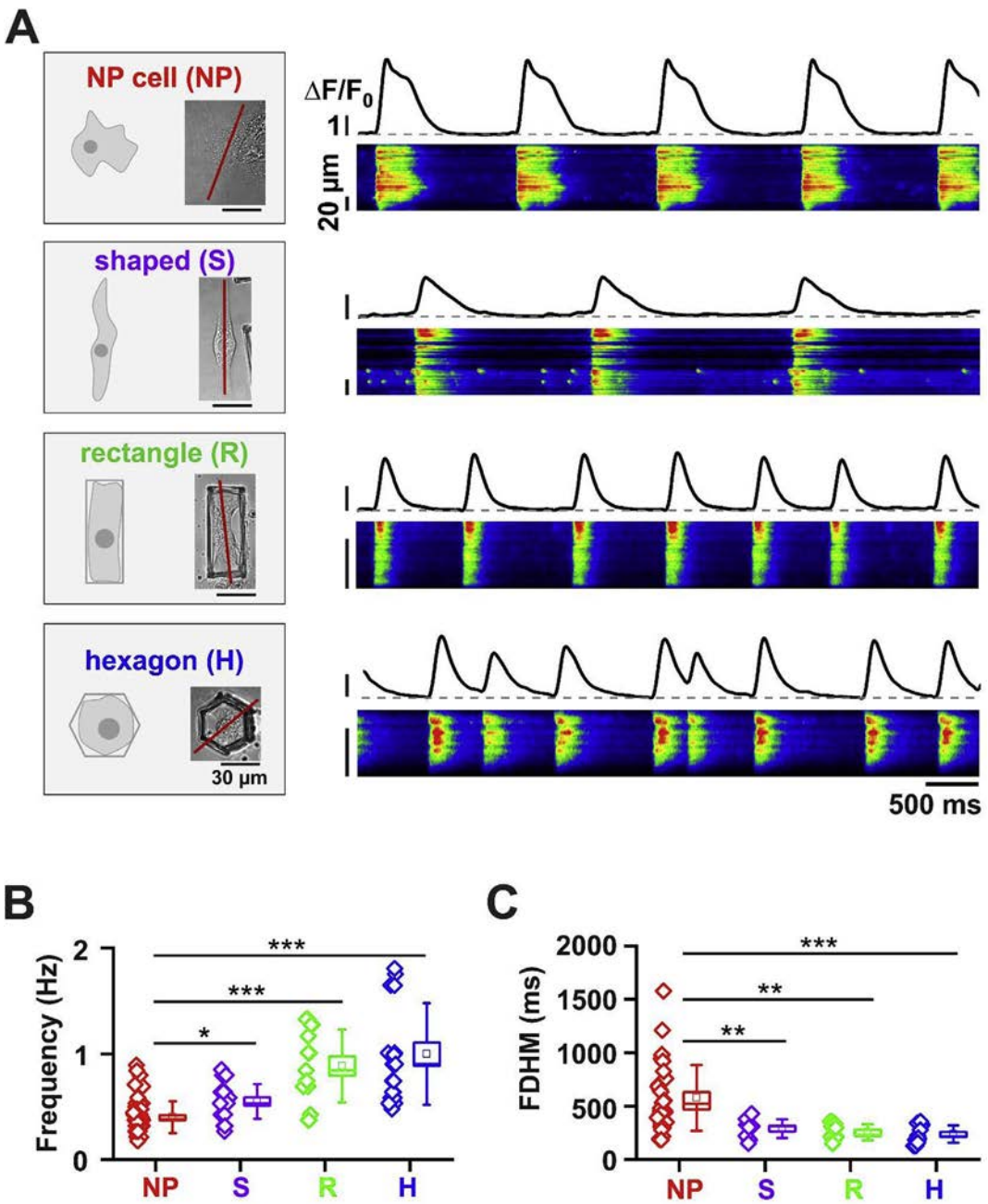

Fig. 5. Analysis of spontaneous Ca^{2+} transients in differently shaped iPSC-CMs. A) Representative linescan images and corresponding plot profiles of spontaneous Ca^{2+} release events and Ca^{2+} transients in an NP cell, shaped cell, and cells growing either in a rectangular or hexagonal 3D-scaffold. Please note the different Ca^{2+} transient morphologies depending on the cell shape. **B)** Statistical analysis of the frequency of spontaneous Ca^{2+} transients for NP iPSC-CMs (NP: 0.40 ± 0.02 Hz, n = 67, *red*), shaped cells with long axis formation (S: 0.55 ± 0.04 Hz, n = 18, *purple*), cells growing in rectangles (R: 0.89 ± 0.09 Hz, n = 15, *green*) and hexagons (H: 1.00 ± 0.11 Hz, n = 19, *blue*). **C)** Evaluation of FDHM of Ca^{2+} transients in NP iPSC-CMs (NP: 577 ± 53 ms, n = 34, *red*), shaped (S: 288 ± 27 ms, n = 11, *purple*), rectangular (R: 255 ± 11 ms, n = 11, *green*) and hexagonal cells (H: 238 ± 22 ms, n = 14, *blue*) revealed significantly faster Ca^{2+} reuptake dynamics in differently shaped cells versus NP cells.

a significantly slower rise of intracellular Ca^{2+} as evaluated by the time constant τ than R or H cells (Fig. 6H). In addition, NP cells also showed a higher variability reflecting the high degree of heterogeneity and immaturity of these cells in comparison to cells in 3D scaffolds, which displayed significantly reduced coefficients of variation (C_{var} = 0.61 in NP cells vs. 0.34 and 0.36 in R and H cells, respectively). Similar to the tendency of spontaneous Ca^{2+} transients, FDHM of triggered Ca^{2+} transients was significantly shorter in 3D shaped compared to NP cells (Fig. 6I). To assess the relationship of Ca^{2+} released during pacing and total SR Ca^{2+} content, fractional release was calculated from peak caffeine induced Ca^{2+} transient and peak Ca^{2+} transient amplitudes. There was no difference in fractional release between the different cell shapes, which amounted in average to ~75% (Fig. 6J). Finally, the decay kinetics of the triggered Ca^{2+} transients (k_{System}, Fig. 6K) and the caffeine induced Ca^{2+} transients ($k_{Caffeine}$, Fig. 6L) were evaluated by measuring the decay time constant k by a monoexponential fit. While k_{System} comprises functional contribution of SERCA and NCX activity during Ca^{2+} removal, $k_{Caffeine}$ mainly mirrors the activity of the NCX. Therefore, SERCA contribution to the decay kinetics was calculated by the difference of k_{System} and $k_{Caffeine}$. The results revealed a significant increase in SERCA activity in R and H cells grown in 3D scaffolds (**Fig. 6M**). These data fit very well to the general observation that Ca^{2+}

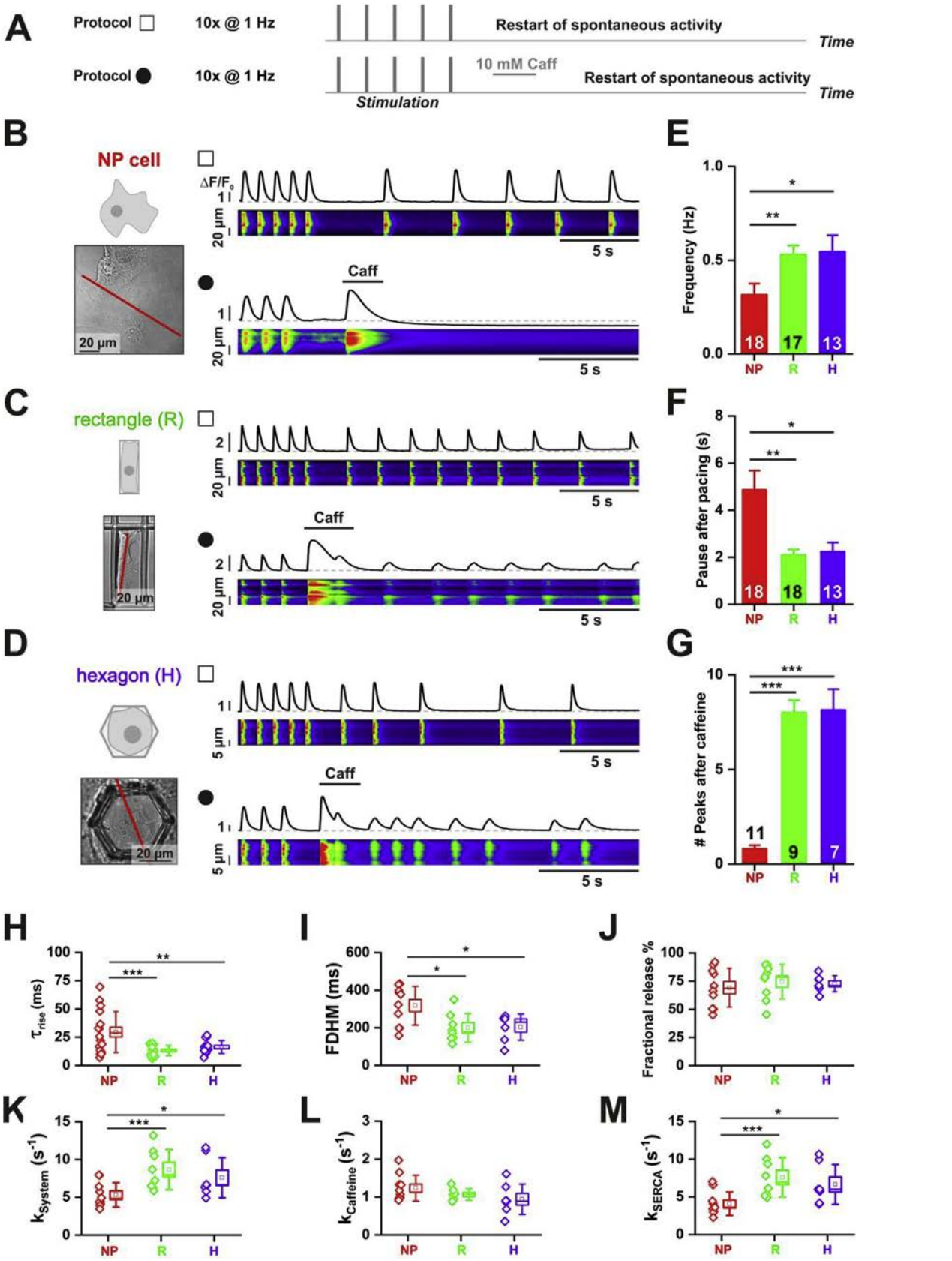

(caption on next page)

Fig. 6. Ca^{2+} handling in stimulated iPSC-CMs. A) Illustration of two stimulation protocols for the analysis of restart of spontaneous activity after stimulation (□) and after SR Ca^{2+} depletion with caffeine (●). Protocol □ included 10 stimulations at 1 Hz, 20 mV. Linescans were recorded starting from the 6th stimulation and at rest for 20 s to record spontaneous activity. In protocol ● application of 10 mM caffeine triggered total SR Ca^{2+} release. **B-D)** Sample linescans and line profiles of an NP cell (**B**) and cells in a cuboid (**C**) or a hexagonal 3D-scaffold (**D**) using both stimulation protocols □ and ●. **E)** Frequency analysis of spontaneous Ca^{2+} transients after stimulation during rest. NP cells showed slower frequency (NP: 0.32 ± 0.06 Hz, n = 18) in comparison to cells in rectangles (R: 0.53 ± 0.05 Hz, n = 17) or hexagons (H: 0.55 ± 0.09 Hz, n = 13). **F)** Analysis of the time after pacing until restart of spontaneous activity revealed significantly longer pause in NP iPSC-CMs (4.86 ± 0.82 s, n = 18) compared with R cells (2.09 ± 0.24 s, n = 18) and H cells (2.24 ± 0.39 s, n = 13). **G)** Number of Ca^{2+} transients after caffeine application during linescan acquisition: NP cells revealed fewer Ca^{2+} transients (0.8 ± 0.2, n = 11) compared with R cells (8.0 ± 0.7, n = 9) and H cells (8.1 ± 1.1, n = 7). **H)** Time constant of rise of triggered Ca^{2+} transients in R cells (13.2 ± 1.1 ms, n = 18) and H cells (16.2 ± 1.6 ms, n = 14) showed significantly faster τ than NP cells (29.5 ± 4.3 ms, n = 18). **I)** Analysis of FDHM of triggered Ca^{2+} transients revealed faster reuptake mechanisms in R and H cells compared with NP cells. **J)** Fractional release was not different in the three growth conditions and amounted to 69 ± 5% in NP cells (n = 10), 74 ± 5% in R cells (n = 9) and 73 ± 3% in H cells (n = 7). **K-M)** Decay time constants of triggered Ca^{2+} transients (**K**), caffeine-induced Ca^{2+} transients (**L**) and SERCA-dependent contribution to decay rate (**M**) revealed significant increase in SERCA activity in cells grown in 3D-scaffolds.

transients have longer duration in NP cells. Most importantly, our quantitative analysis of Ca^{2+} transient kinetics demonstrates that during structural remodeling in 3D scaffolds, a significant maturation of the Ca^{2+} handling processes takes place, especially regarding Ca^{2+} release (τ_{rise}) and reuptake dynamics (k_{SERCA}).

4. Discussion

During cardiac development, numerous environmental cues influ ence the structural and functional maturation processes that lead to the complex phenotype of adult cardiomyocytes [5,23]. Regular pumping activity comprising the periodic switch between contraction and re laxation, mechanical load that induces passive stretch on cells, stimu lating signals from pacemaker cells that synchronize electrical and contractile activity, and humoral regulation by neighboring vascular endothelial cells, fibroblasts as well as systemic activity are only some of the mechanisms that have been identified to impact on cardiomyo cyte maturation [4,24 27]. These are part of the difficulties that re searchers are confronted with when cardiomyocytes are produced from pluripotent cells. After successful differentiation, an immature cardio myocyte phenotype is maintained, and it has yet not been possible to maturate iPSC CMs showing adult characteristics *in vitro*, as it is basi cally impossible to reproduce the natural conditions in a culture system. The main goal of this work was to investigate the impact of structural changes on one of the key aspects of cardiomyocyte function, namely the control of Ca^{2+} homeostasis.

4.1. Structural remodeling of iPSC CMs in 3D scaffolds

In contrast to the cuboid like structure of adult ventricular cardio myocytes, iPSC CMs grown on a planar surface do not naturally take the form of adult cells, but stay rather flat with unspecific cell shape. This might be attributable to the absence of cell neighbors in 3D and con sequently also to the lack of directed activity during contraction. In our experimental approach, we have tested the hypothesis that structural alteration of iPSC CM shape influences cellular and subcellular micro architecture. Single cells were forced to grow in rectangular shaped 3D scaffolds and the consequences of structural remodeling were in vestigated. In this novel cell culture setup, the scaffold walls served not only as size limitation for cell growth and expansion, but additionally as contact points for myocyte attachment. Our data demonstrate that growth in the shape of a cuboid leads to the formation of a long cell axis with strict parallel alignment of myofibrils. This novel arrangement of the contractile apparatus resembles the organization in adult cardio myocytes, as shown by the pattern of α actinin distribution. Reorganization of myofibrils along the cell's long axis has strong impact on the contractile behavior of the cell as contraction along only one axis might enhance contraction amplitude and consequently force produc tion [28]. Similar findings have been described before and confirm the structural reorganization of iPSC CMs on 2D patterned substrates [29]. In the study of *Ribeiro* et al., the authors have investigated especially the biomechanical properties of stem cell derived cardiomyocytes on 2D printed rectangular patterns of different aspect ratios. Myofibril align ment resulted in more mature sarcomere organization and strengthened adhesion to the substrate at the cell extremities. In contrast, in the present study we used 3D micro scaffolds to investigate the effect of reshaping single cells in a rectangular 3D environment. In this model, single cells have the possibility to adhere not only to the bottom sur face, but also to the surrounding scaffold walls (which are equally covered with extracellular matrix proteins). Our structural analysis demonstrates that restriction of planar growth leads to increase in cell height resulting in significant remodeling of subcellular structures. The gain in 3D space may not only allow rearrangement of myofibrils and organelles, but also alter diffusional space and dynamics for local and global Ca^{2+} release events. Our structural analysis has further revealed that the expression pattern of RyR2 changed from a dotted distribution in unshaped and hexagonal cells to a strong and regular striation pat tern in rectangular shaped cells. The distribution pattern of RyR2 is indicative of a rearrangement of the SR from a disordered tubule system to an organized subcellular membrane network oriented along myofi brils. This new expression pattern of RyR2 is an important step towards maturation of the Ca^{2+} handling apparatus for efficient contractions as it brings the main Ca^{2+} release channel, and thus the activating Ca^{2+}, into close proximity to the myofibrils [30,31].

Another critical difference in the morphology between immature and mature cardiomyocytes is directly related to the function of EC coupling: in addition to the specific outer shape of adult myocytes, their well organized network of t tubules located near the sarcomeric Z plane functionally couples to the SR to form dyads, which serve as structural basis for efficient CICR [32,33]. So far, natural development of an orderly t tubule network has not been described in iPSC CMs [13]. Here, we have investigated the membrane outline and found no membrane invaginations in NP iPSC CMs. However, in cells grown in 3D micro scaffolds, we repeatedly found membrane tubules that pro truded inwards deep into the cell. Most prominent in rectangular shaped cells, these membrane projections preferentially developed at the cell poles, but also projected from the cell surface into the cell as indicated in the top view of our images. This observation suggests that the spatial limitation of cell expansion and the related increase in cell height may trigger tubule formation. Currently, we can imagine three scenarios to resolve the underlying mechanisms, which may be even intimately linked to each other: 1.) The increase in cell height during growth within the scaffold results in a larger cell thickness, which might create a new need of the inner subcellular space and densely packed compartments to develop membrane invaginations distances deep into the cell for better signaling, enhanced supply with electrolytes and nutrients, and reduction of diffusion, which is not required in very flat cells with a naturally greater surface volume ratio. 2.) Wall adhesion may increase passive stretch of the cell membrane during contraction and activate mechanosensitive pathways, possibly ion channels of the TRP family. Channel activity may activate intracellular signaling cas cades to switch on certain gene programs for structural remodeling. 3.) Mechanosensation may be conveyed by integrin receptor signaling pathways and activate outside in signaling pathways to initiate

structural remodeling processes. Previously, the formation of a primi tive t tubular network has only been achieved by overexpression of Bin 1, a protein required for membrane invagination and tubule formation in striated muscle cells [34,35]. In a recent report, Bin 1 overexpression induced strong membrane tubules in embryonic stem cell derived car diomyocytes with strong impact on the expression patterns of $Ca_v1.2$ and RyR2 [36]. So far, we can only speculate about the processes in volved in the formation of t tubules, but it will be an interesting task to investigate the putative mechanisms. Here, our data demonstrate for the first time that it is sufficient to reshape iPSC CMs in 3D micro scaffolds to induce tubule formation with positive consequences on the structural and functional maturation of Ca^{2+} handling mechanisms. The development of a t tubule like membrane network was further confirmed by ultrastructural analysis, which revealed regularly ordered tubules in direct vicinity of the sarcomeric Z disc in rectangular shaped iPSC CMs. Furthermore, immunostainings uncovered strong re organization of $Ca_v1.2$ and RyR2 relative to each other leading to co distribution of both Ca^{2+} channels in the appearance of a striated pattern suggestive of dyad formation as in mature cardiomyocytes. Positioning of sarcolemmal membrane (containing $Ca_v1.2$) and SR tu bules (expressing RyR2) near to myofibrils has important functional consequences, since the Ca^{2+} regulating machinery needed for a pre cise control of contraction is directly positioned to the place of action.

4.2. Functional remodeling of Ca^{2+} handling in reshaped iPSC CMs

From disease conditions, we have learnt that cardiac function strictly depends on structure and that pathophysiological structural remodeling as for example in cardiac hypertrophy has severe con sequences on EC coupling leading to reduced coupling efficiency be tween $Ca_v1.2$ and RyR2 [37 40]. In developing cardiomyocytes, the missing precise microarchitecture results in similar differences in Ca^{2+} handling compared to healthy and mature cardiomyocytes [41 43]. One hallmark of immaturity in iPSC CMs is the spontaneous beating activity and the high propensity for spontaneous Ca^{2+} release events. The mechanisms underlying automaticity have not yet been fully elu cidated. However, the concept of a concerted interplay between the membrane clock (describing the interplay of depolarizing and re polarizing ion channels) and the Ca^{2+} clock (comprising the sponta neous Ca^{2+} release and Ca^{2+} removal machinery) mechanisms may deliver the most probable explanation for the development of sponta neous contractions [44,45]. The strong expression of IP_3Rs in iPSC CMs is another important indicator for an immature phenotype. In adult ventricular cardiomyocytes, the IP_3R is mainly expressed in the nuclear envelope and probably responsible for excitation transcription coupling rather than EC coupling, while in premature native cardiomyocytes, IP_3R is expressed throughout the cell [46]. In iPSC CMs, it is possible that IP_3Rs may be involved in the development of spontaneous Ca^{2+} release events and help to sustain the oscillatory activity. However, the role of IP_3R mediated Ca^{2+} signaling in iPSC CMs remains to be elu cidated in specific experiments.

iPSC CMs express all relevant Ca^{2+} handling proteins that are in volved in Ca^{2+} influx, cytosolic Ca^{2+} release and Ca^{2+} removal (our data and [46,47]). Our experiments demonstrate that in NP cells, spontaneous Ca^{2+} release is characterized by low frequency and slow Ca^{2+} removal mechanisms as indicated by the long lasting Ca^{2+} tran sient duration. Reshaping iPSC CMs leads to significantly higher fre quencies of spontaneous Ca^{2+} transients and faster Ca^{2+} recycling after release. The differences in spontaneous beating frequencies and Ca^{2+} handling properties between NP and 3D shaped iPSC CMs were also confirmed by measuring the spontaneous Ca^{2+} release characteristics after a series of triggered Ca^{2+} transients and emptying the SR Ca^{2+} store by caffeine application. In all conditions, 3D shaped iPSC CMs revealed significantly stronger Ca^{2+} handling mechanisms as indicated by early and robust recovery after caffeine dependent Ca^{2+} release and higher frequency of spontaneous beats. At first sight, it may appear counter intuitive to have higher beating frequency as a result of ma turation processes. However, this increase may have to be interpreted as an improvement of overall Ca^{2+} handling during the Ca^{2+} release reuptake cycles. Only optimal SR Ca^{2+} reloading will provide sufficient Ca^{2+} for the next release [48]. Therefore, picking up in speed may be seen as the result of more efficient Ca^{2+} recycling and a first step to wards Ca^{2+} signaling maturation.

In line with our findings on spontaneous Ca^{2+} release character istics, analysis of electrically triggered Ca^{2+} transients also revealed faster Ca^{2+} release and reuptake mechanisms in 3D shaped iPSC CMs compared with NP cells. In line with the recent demonstration of en hanced Ca^{2+} transients in Bin 1 overexpressing ESC CMs [36], espe cially the faster rising phase of Ca^{2+} transients in our measurements may indicate an increase in the coupling efficiency between $Ca_v1.2$ and RyR2. These functional data fit very well to our structural findings that especially in rectangular shaped iPSC CMs, reorganization of the ex pression pattern of $Ca_v1.2$ and RyR2 leads to enhanced spatial clus tering of both Ca^{2+} channels, the basis for increased CICR. In future studies, it will be interesting to use these novel 3D micro scaffolds for detailed electrophysiological investigations of the development and maturation of the EC coupling mechanism in reshaped iPSC CMs.

In addition, this is the first study that demonstrates faster decay of the Ca^{2+} transient in 3D shaped iPSC CMs. Detailed analysis of the kinetics revealed significantly increased SERCA contribution while sarcolemmal Ca^{2+} removal mechanisms were not different. This en hanced SERCA activity after Ca^{2+} release is a direct evidence of im proved Ca^{2+} handling mechanisms in 3D shaped iPSC CMs. Faster Ca^{2+} reuptake into the SR also explains the increased frequency and the robust return to spontaneous beating activity after Ca^{2+} depletion. The fact that we see functional differences between NP and 3D shaped cells indicates that the increase in cell height and thus, the subcellular spatial reorganization is a critical factor in the improvement of Ca^{2+} dynamics in iPSC CMs.

Taken together, this study provides the first experimental evidence that a change in cell structure leads to membrane tubule formation and improved Ca^{2+} handling of iPSC CMs.

Author contributions

N.D.U. and M.B. initiated the study and designed the research, N.D.U. and M.H. supervised the project. N.S. and N.D.U. performed the experiments and data analysis, A.K. and J.B. carried out im munostainings. M.J., S·B., B.R., M.H. and M.B. designed and prepared the scaffolds, A.H. performed electron microscopy. N.S. and N.D.U. wrote the first draft of the manuscript. All authors discussed the results and completed the manuscript.

Data availability

The raw/processed data required to reproduce these findings cannot be shared at this time due to technical or time limitations.

Declaration of competing interest

The authors declare no competing interests.

Acknowledgements

We thank Manuela Höfer, Ursula Wald, Michael Bartolf Kopp, Sarawuth Wantha and Tatjana J. Autenrieth for their technical and experimental assistance and Hilmar Bading for the possibility to use the electron microscopy facility. We would particularly like to acknowledge Karin Gorgas for critical reading of the manuscript and Joachim Kirsch for insightful discussions. This work has received funding from the HEiKA Heidelberg Karlsruhe Research Partnership (to N.D.U. and M.B.) and the German Research Council (UL 466/2 1).

References

[1] E. Carvalho, P. Verma, K. Hourigan, R. Banerjee, Myocardial infarction: stem cell transplantation for cardiac regeneration, Regen. Med. 10 (2015) 1025–1043.
[2] B. Fujita, W.-H. Zimmermann, Myocardial tissue engineering strategies for heart repair: current state of the art, Interact. Cardiovasc. Thorac. Surg. 27 (2018) 916–920.
[3] C.L. Mummery, Perspectives on the use of human induced pluripotent stem cell-derived cardiomyocytes in biomedical research, Stem Cell Rep. 11 (2018) 1306–1311.
[4] T.J. Kolanowski, C.L. Antos, K. Guan, Making human cardiomyocytes up to date: derivation, maturation state and perspectives, Int. J. Cardiol. 241 (2017) 379–386.
[5] R. Zhu, A. Blazeski, E. Poon, et al., Physical developmental cues for the maturation of human pluripotent stem cell-derived cardiomyocytes, Stem Cell Res. Ther. 5 (2014) 117.
[6] J.J.H. Chong, X. Yang, C.W. Don, et al., Human embryonic-stem-cell-derived cardiomyocytes regenerate non-human primate hearts, Nat. Nat. Publ. Group 510 (2014) 273–277.
[7] Y. Shiba, S. Fernandes, W.-Z. Zhu, et al., Human ES-cell-derived cardiomyocytes electrically couple and suppress arrhythmias in injured hearts, Nature 489 (2012) 322–325.
[8] M.M. Maleckar, A.G. Edwards, W.E. Louch, G.T. Lines, Studying dyadic structure-function relationships: a review of current modeling approaches and new insights into Ca2+ (mis)handling, Clin. Med. Insights Cardiol. 11 (2017) 1–11.
[9] C. Ferrantini, C. Crocini, R. Coppini, et al., The transverse-axial tubular system of cardiomyocytes, Cell. Mol. Life Sci. 70 (2013) 4695–4710.
[10] D. Bers, Cardiac excitation–contraction coupling, Nature 415 (2002) 198.
[11] C. Crocini, C. Ferrantini, M. Scardigli, et al., Novel insights on the relationship between T-tubular defects and contractile dysfunction in a mouse model of hypertrophic cardiomyopathy, J. Mol. Cell. Cardiol. 91 (2015) 42–51.
[12] C. Crocini, R. Coppini, C. Ferrantini, et al., Defects in T-tubular electrical activity underlie local alterations of calcium release in heart failure, Proc. Natl. Acad. Sci. U.S.A. 111 (2014) 15196–15201.
[13] M. Gherghiceanu, L. Barad, A. Novak, J. Itskovitz-Eldor, L.M. Popescu, Cardiomyocytes derived from human embryonic and induced pluripotent stem cells: comparative ultrastructure, J. Cell Mol. Med. 15 (2011) 2539–2551.
[14] L. Lipskaia, Z. Keuylian, K. Blirando, et al., Expression of sarco (endo) plasmic reticulum calcium ATPase (SERCA) system in normal mouse cardiovascular tissues, heart failure and atherosclerosis, Biochim. Biophys. Acta 1843 (2014) 2705–2718.
[15] O.J. Abilez, E. Tzatzalos, H. Yang, et al., Passive stretch induces structural and functional maturation of engineered heart muscle as predicted by computational modeling, Stem Cells 36 (2017) 265–277.
[16] X. Sun, S.S. Nunes, Bioengineering approaches to mature human pluripotent stem cell-derived cardiomyocytes, Front. Cell Dev. Biol. 5 (2017) 19.
[17] M. Tiburcy, J.E. Hudson, P. Balfanz, et al., Defined engineered human myocardium with advanced maturation for applications in heart failure modeling and repair, Circulation 135 (2017) 1832–1847.
[18] V. Sottas, C.-M. Wahl, M.C. Trache, et al., Improving electrical properties of iPSC-cardiomyocytes by enhancing Cx43 expression, J. Mol. Cell. Cardiol. 120 (2018) 31–41.
[19] N.D. Ullrich, H.H. Valdivia, E. Niggli, PKA phosphorylation of cardiac ryanodine receptor modulates SR luminal Ca2+ sensitivity, J. Mol. Cell. Cardiol. 53 (2012) 33–42.
[20] A. Schaap, Y. Bellouard, Molding topologically-complex 3D polymer microstructures from femtosecond laser machined glass, Opt. Mater. Express 3 (2013) 1428.
[21] K.C. Richardson, L. Jarett, E.H. Finke, Embedding in epoxy resins for ultrathin sectioning in electron microscopy, Stain Technol. 35 (1960) 313–323.
[22] M.E. Díaz, S.C. O'Neill, D.A. Eisner, Sarcoplasmic reticulum calcium content fluctuation is the key to cardiac alternans, Circ. Res. 94 (2004) 650–656.
[23] A. Di Maio, K. Karko, R.M. Snopko, R. Mejía-Alvarez, C. Franzini-Armstrong, T-tubule formation in cardiacmyocytes: two possible mechanisms? J. Muscle Res. Cell Motil. 28 (2007) 231–241.
[24] K. Kroll, M. Chabria, K. Wang, et al., Electro-mechanical conditioning of human iPSC-derived cardiomyocytes for translational research, Prog. Biophys. Mol. Biol. 130 (2017) 212–222.
[25] J.B. Freund, J.G. Goetz, K.L. Hill, J. Vermot, Fluid flows and forces in development: functions, features and biophysical principles, Development 139 (2012) 1229–1245.
[26] P. Pandey, W. Hawkes, J. Hu, et al., Cardiomyocytes sense matrix rigidity through a combination of muscle and non-muscle myosin contractions (vol 44, pg 326, 2018), Dev. Cell 45 (2018) 661–661.
[27] K.E. Sullivan, L.D. Black, The role of cardiac fibroblasts in extracellular matrix-mediated signaling during normal and pathological cardiac development, J. Biomech. Eng. 135 (2013) 71001.
[28] N. Hampe, T. Jonas, B. Wolters, et al., Defined 2-D microtissues on soft elastomeric silicone rubber using lift-off epoxy-membranes for biomechanical analyses, Soft Matter 10 (2014) 2431.
[29] A.J.S. Ribeiro, Y.-S. Ang, J.-D. Fu, et al., Contractility of single cardiomyocytes differentiated from pluripotent stem cells depends on physiological shape and substrate stiffness, Proc. Natl. Acad. Sci. U.S.A. 112 (2015) 12705–12710.
[30] F. Hiess, A. Vallmitjana, R. Wang, et al., Distribution and function of cardiac ryanodine receptor clusters in live ventricular myocytes, J. Biol. Chem. 290 (2015) 20477–20487.
[31] P. Asghari, M. Schulson, D.R.L. Scriven, G. Martens, E.D.W. Moore, Axial tubules of rat ventricular myocytes form multiple junctions with the sarcoplasmic reticulum, Biophys. J. 96 (2009) 4651–4660.
[32] X.H. Sun, F. Protasi, M. Takahashi, H. Takeshima, D.G. Ferguson, C. Franzini-Armstrong, Molecular architecture of membranes involved in excitation-contraction coupling of cardiac muscle, J. Cell Biol. 129 (1995) 659–671.
[33] M.L. Munro, C. Soeller, Early transverse tubule development begins in utero in the sheep heart, J. Muscle Res. Cell Motil. 37 (2016) 195.
[34] J.L. Caldwell, C.E. Smith, R.F. Taylor, et al., Dependence of cardiac transverse tubules on the BAR domain protein amphiphysin II (BIN-1), Circ. Res. 115 (2014) 986–996.
[35] T. Hong, J.W. Smyth, D. Gao, et al., BIN1 localizes the L-type calcium channel to cardiac T- tubules, PLoS Biol. 8 (2010) e1000312.
[36] A. La Mata De, S. Tajada, S. O'Dwyer, et al., BIN1 induces the formation of T-tubules and adult-like Ca2+ release units in developing cardiomyocytes, Stem Cells 37 (2018) 54–64.
[37] M.B. Cannell, D.J. Crossman, C. Soeller, Effect of changes in action potential spike configuration, junctional sarcoplasmic reticulum micro-architecture and altered t-tubule structure in human heart failure, J. Muscle Res. Cell Motil. 27 (2006) 297–306.
[38] S.M. Bryant, C.H.T. Kong, J.J. Watson, et al., Caveolin 3-dependent loss of t-tubular I-Ca during hypertrophy and heart failure in mice, Exp. Physiol. 103 (2018) 652–665.
[39] A.M. Gómez, H.H. Valdivia, H. Cheng, et al., Defective excitation-contraction coupling in experimental cardiac hypertrophy and heart failure, Science 276 (1997) 800–806.
[40] J.-P. Benitah, B.G. Kerfant, G. Vassort, S. Richard, A.M. Gómez, Altered communication between L-type calcium channels and ryanodine receptors in heart failure, Front. Biosci. 7 (2002) e263–e275.
[41] D.H. Jung, C.J. Lee, C.K. Suh, H.J. You, Molecular properties of excitation-contraction coupling proteins in infant and adult human heart tissues, Mol. Cells 20 (2005) 51–56.
[42] S.A. McDowell, E. McCall, W.F. Matter, T.B. Estridge, C.J. Vlahos, Phosphoinositide 3-kinase regulates excitation-contraction coupling in neonatal cardiomyocytes, Am. J. Physiol. Heart Circ. Physiol. 286 (2003) H796–H805.
[43] M. Zaccolo, T. Pozzan, Discrete microdomains with high concentration of cAMP in stimulated rat neonatal cardiac myocytes, Science 295 (2002) 1711–1715.
[44] T.M. Vinogradova, S.T. Sirenko, E.G. Lakatta, Unique Ca2+-cycling protein abundance and regulation sustains local Ca2+ releases and spontaneous firing of rabbit sinoatrial node cells, Int. J. Mol. Sci. 19 (2018) 8.
[45] E.G. Lakatta, V.A. Maltsev, T.M. Vinogradova, A coupled SYSTEM of intracellular Ca2+ clocks and surface membrane voltage clocks controls the timekeeping mechanism of the heart's pacemaker, Circ. Res. 106 (2010) 659–673.
[46] I. Itzhaki, S. Rapoport, I. Huber, et al., Calcium handling in human induced pluripotent stem cell derived cardiomyocytes, PLoS One 6 (2011) e18037.
[47] Y.-K. Lee, K.-M. Ng, W.-H. Lai, et al., Calcium homeostasis in human induced pluripotent stem cell-derived cardiomyocytes, Stem Cell Rev. 7 (2011) 976–986.
[48] J. Liu, J.-D. Fu, C.-W. Siu, R.A. Li, Functional sarcoplasmic reticulum for calcium handling of human embryonic stem cell-derived cardiomyocytes: insights for driven maturation, Stem Cells 25 (2007) 3038–3044.
[49] C. Pasqualin, F. Gannier, C.O. Malécot, P. Bredeloux, V. Maupoil, Automatic quantitative analysis of t-tubule organization in cardiac myocytes using ImageJ, AJP. Cell Physiol. 308 (2015) C237–C245.
[50] M.A. Bray, S.P. Sheehy, K.K. Parker, Sarcomere alignment is regulated by myocyte shape, Cell Motil. Cytoskelet. 65 (8) (2008) 641–651.